

# Resource-Conscious RL Algorithms for Deep Brain Stimulation

Arkaprava Gupta  
 Dept. of Computer Science  
 UNC Chapel Hill  
 USA

Prateek Ganguli  
 Dept. of Computer Science  
 UNC Chapel Hill  
 USA

Parasara Sridhar Duggirala  
 Dept. of Computer Science  
 UNC Chapel Hill  
 USA

Nicholas Carter  
 Dept. of Computer Science  
 UNC Chapel Hill  
 USA

Benedikt Dietrich  
 Hochschule München  
 Germany, USA

William Zellers  
 Dept. of Computer Science  
 UNC Chapel Hill  
 USA

Vibhor Krishna  
 Dept. of Neurosurgery  
 UNC Chapel Hill  
 USA

Samarjit Chakraborty  
 Dept. of Computer Science  
 UNC Chapel Hill  
 USA

## Abstract

Deep Brain Stimulation (DBS) has proven to be a promising treatment of Parkinson's Disease (PD). DBS involves stimulating specific regions of the brain's Basal Ganglia (BG) using electric impulses to alleviate symptoms of PD such as tremors, rigidity, and bradykinesia. Although most clinical DBS approaches today use a fixed frequency and amplitude, they suffer from side effects (such as slurring of speech) and shortened battery life of the implant. Reinforcement learning (RL) approaches have been used in recent research to perform DBS in a more adaptive manner to improve overall patient outcome. These RL algorithms are, however, too complex to be trained *in vivo* due to their long convergence time and requirement of high computational resources.

We propose a new *Time & Threshold-Triggered Multi-Armed Bandit* (T3P MAB) RL approach for DBS that is more effective than existing algorithms. Further, our T3P agent is lightweight enough to be deployed in the implant, unlike current deep-RL strategies, and even forgoes the need for an offline training phase. Additionally, most existing RL approaches have focused on modulating only frequency or amplitude, and the possibility of tuning them together remains greatly unexplored in the literature. Our RL agent can tune both frequency and amplitude of DBS signals to the brain with better sample efficiency and requires minimal time to converge. We implement an MAB agent for DBS for the first time on hardware to report energy measurements and prove its suitability for resource-constrained platforms. Our T3P MAB algorithm is deployed on a variety of microcontroller unit (MCU) setups to show its efficiency in terms of power consumption as opposed to other existing RL approaches used in recent work.

## 1 Introduction

Around 930,000 people in the U.S. currently suffer from Parkinson's Disease (PD) with 1,238,000 being the projected number by the year 2030 [20]. Patients with PD commonly suffer from motor symptoms like tremors, rigidity, slowness of movement and postural instability. Deep brain stimulation (DBS) has proven to be a promising technique for the treatment of PD and is widely used today to alleviate motor symptoms in PD patients. Approximately 10,000 DBS implant surgeries are performed in the U.S. every year. This procedure involves

stimulating specific sites within the Basal Ganglia (BG) with electrical signals through an implantable device. This implant consists of a pulse generator and an electrode. The pulse generator is a battery-powered device responsible for generating the train of electrical pulses and is usually implanted under the skin near the collarbone. These pulses are delivered to the brain through the electrode, connected to the pulse generator by means of an insulated wire. The electrode is carefully placed inside the brain, with the tip at the specific site of the BG region. Fig. 1 provides an overview of this setup.

**Types of DBS:** Most modern clinical approaches use continuous DBS (cDBS) that involves stimulating the brain of the patient with a fixed amplitude and frequency. Patients must visit their neurologist multiple times a year so that the frequency of stimulations can be tuned to best fit their health needs. The effectiveness of stimulation is typically evaluated by monitoring neural activity in the brain regions affected by Parkinson's disease, particularly those involved in motor control.

In conventional setups, the strength of beta-band activity ( $P_\beta$ ) is measured from local field potentials (LFPs) recorded in the globus pallidus internus (GPI) region of the brain. LFPs are recordings of the collective electrical activity of neurons that can be sensed via the implant.  $P_\beta$  serves as a biomarker to guide the adjustment of DBS frequency in clinical setups. Details on the  $P_\beta$  biomarker are given later in Section 3. This approach, however, suffers from energy inefficiency [16] and may cause unwanted side effects such as speech slurring. This has led to many works that focus on adaptive DBS (aDBS), which adjusts the stimulation based on the current state of the brain. aDBS is known to reduce side effects from stimulation while being energy efficient [6, 29]. Some commercial devices for aDBS exist, with most of them using either rule-based or SVM-driven control policies to adjust stimulation parameters.

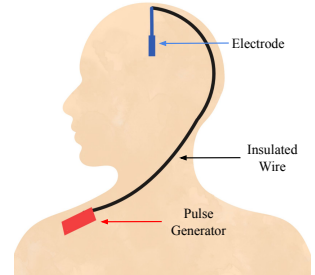


Figure 1: Deep Brain Stimulation

**aDBS Limitations:** Existing aDBS approaches have several limitations. Most approaches rely on deep-RL agents, which require an extensive offline training phase because they are too resource-intensive to run directly on the implant, as they rely on training neural networks. In offline training, patient data is collected from the implant and is used to train the deep-RL algorithms in simulations. The neural networks used in deep-RL algorithms also make the underlying decision process opaque, reducing interpretability and trustworthiness in clinical settings. Furthermore, these algorithms are computationally expensive, leading to higher energy consumption and shortened battery life. Another drawback is their lack of flexibility. Deep-RL policies are difficult to modify so that feedback from the clinician and/or the patient is included in the decision making algorithm. As PD progresses, the underlying neural patterns change, causing previous training data to become outdated and necessitating retraining of the RL agent. Currently, commercially available aDBS devices also still need a calibration phase to personalize the stimulation parameter for each patient, as is required for deep-RL approaches, further increasing the burden on both clinicians and patients.

**Our proposal:** In order to alleviate these problems, we present a Multi-Armed Bandit (MAB) approach denoted the **Time & Threshold-Triggered Pruned Multi-Armed Bandit (T3P MAB)** algorithm for DBS which is transparent and easier for the neurologist to understand and modify. It is efficient in terms of energy consumption and can be implemented *in vivo* without the need for a prior offline training phase. MABs are a class of RL algorithms that do not model state transitions. They find the optimal action using observed rewards in the current state without the need for neural networks and are therefore lightweight in terms of computation. In our experiments, the T3P MAB agent demonstrates better performance with respect to both existing MAB and deep-RL approaches in suppressing PD symptoms. Notably, our MAB approach also uses less power for stimulation during this compared to deep-RL strategies. This is in addition to the advantage of sample efficiency, in contrast to deep-RL algorithms which require a huge amount of training data.

**μC implementations:** We deployed our T3P MAB algorithm on the ESP32-S3 and ESP32-P4 microcontroller units (MCUs) and report power and energy consumption measurements using a high-precision real-time power analyzer. Our implementation is further compared against existing commercial DBS devices in terms of power consumption characteristics. To our knowledge, this is the first work that deploys an MAB algorithm for DBS in hardware to report power metrics. Our work advances the state-of-the-art in personalized medicine by minimizing the need for human intervention in regulating stimulation parameters while also ensuring symptoms suppression, with enough power-efficiency to be suitable for implantable hardware. Although MAB algorithms require a convergence time before the patient is stabilized, this duration is small, typically under 2 minutes as observed in our experiments.

**Summary of contributions:** Our work consists of the following:

- (1) We propose our **T3P MAB** algorithm to explore the possibility of modulating amplitude and frequency for DBS, an approach which has not been explored extensively in literature.

- (2) We compare the T3P MAB algorithm with other MAB approaches, as well as existing deep-RL approaches to show that our algorithm more effectively suppresses the  $P_\beta$  biomarker and reduces DBS stimulation energy consumption more than the state-of-the-art deep-RL methods, with remarkable sample efficiency.
- (3) We implement an MAB RL approach in hardware for the first time in the context of DBS and report detailed energy metrics. We further compare this implementation with both existing deep-RL methods and existing devices for DBS.

**Organization of the paper:** Our work is contrasted against recent work in Section 2. In Section 3, we introduce the details of the BGT model and discuss a variety of popular MAB algorithms. Section 4 proposes the problem formulation for MAB and the design of the reward function. Results are discussed in Section 5, where we compare the MAB algorithms with existing deep RL algorithms in terms of effectiveness and energy efficiency. We conclude the paper and discuss future work in Section 6.

## 2 Related Work

Recent work has explored the possibility of using RL techniques to design effective strategies to perform aDBS with most of them relying on deep-RL approaches [4, 5, 7–9, 19]. A majority of these only consider frequency modulation for DBS while the possibility of modulating amplitude, or both amplitude and frequency, has been left relatively unexplored [5, 10]. Further, the use of MAB has not been sufficiently explored in the domain of DBS and only recently have some results on the use of MAB in restricted settings been reported [12]. In contrast to these studies, where only the frequency of the stimulation has been adapted, we show that MAB can be successfully used for a more complete joint frequency and amplitude modulation.

A recent study compares various deep-RL algorithms used for DBS and finds the Twin Delayed Deep Deterministic Policy Gradient (TD3) algorithm to be superior to the others in terms of suppressing the  $P_\beta$  biomarker [5]. We used an implementation of the TD3 agent from a recent work [4] to draw a comparative study against our MAB approach. We also compare our algorithm against other MAB algorithms, along with the one proposed in [12] for frequency modulation only. The experiments are performed on a model of the human brain, that simulates both healthy and PD conditions, which has been refined through multiple works over the years [13, 22, 23, 26]. Although RL has not been adopted into commercial devices yet, a recent work performs experiments on real patients to prove that the use of RL is indeed a promising direction of work [10].

## 3 Preliminaries

In this section, we first describe the Basal Ganglia-Thalamic (BGT) model. The biomarkers used for testing effectiveness of DBS on the BGT model are discussed thereafter. Next, we discuss MAB as an RL algorithm and some of the popular MAB approaches that we use in our experiments. Finally, we discuss deep RL strategies and elaborate on the TD3 approach that has been frequently used in recent DBS research for PD.

### 3.1 The Basal Ganglia-Thalamic (BGT) Model

Due to the inherent complexities of testing black box neural network algorithms tasked with critical decision making on live human brains, we utilize a computational brain model [23]. More specifically, it models the BG and thalamus regions of the brain, as they are the most affected by PD. Additionally, the model is capable of simulating PD afflicted brain activity in addition to baseline neural activity. Several works have improved this model over the years [22, 26], and we use the most recent one given in [13]. The BGT model allows for simulation of voltage spiking activity of individual neurons of the globus pallidus internus (GPI), the globus pallidus externus (GPe), and the subthalamic nucleus (STN) regions found within the BG, as well as the thalamus (TH) region. A block diagram representation of the BGT model along with our setup is shown in Fig. 2.

The regions in green indicate regions of the BG that are part of our brain model, and the other regions in blue are ones that are not part of the BG but we include them in our model for a more realistic simulation of the human brain. As mentioned before, local field potentials (LFPs) can be obtained from the GPI region of the brain for calculation of the  $P_\beta$  biomarker, which allows us to observe the current state of the brain. The  $P_\beta$  is an important biomarker which is used by most of the state-of-the-art implementations of DBS algorithms today, not only in research but also in implants in the real patients. Similarly, the error index (EI) biomarker can be obtained from the TH region. We discuss both of these biomarkers in more detail at the end of this section. The deep brain stimulator is the device that resides in the human body which is responsible for sending impulses to the STN region of the brain to stabilize the patient. Although stimulating and sensing at different regions is not yet common in clinical practice, our setup is inspired by recent works that predominantly use this approach [5, 7, 12]. This configuration can further provide insights into performing DBS in the STN while sensing in the GPI using two different electrodes. Dealing with noise from sensing is a major problem in this domain. By separating sensing and stimulation, we might be able to offer more stable biomarkers for sensing and, therefore, deliver more effective stimulation. In our setup, an RL algorithm resides in this component that senses the current state of the brain using the aforementioned biomarker(s) and updates the stimulation parameters (frequency and amplitude in our case) adaptively.

The neural activity of each region is determined by a myriad of differential equations. The four main equations governing each region are listed below:

$$\begin{aligned} C_m \frac{dv_{STN}}{dt} &= -I_L - I_{Na} - I_K - I_T - I_{Ca} - I_{AHP} \\ &\quad - I_{GPe} + I_{app} + I_{DBS}(t), \\ C_m \frac{dv_{GPe/i}}{dt} &= -I_L - I_{Na} - I_K - I_T - I_{Ca} - I_{AHP} \\ &\quad - I_{STN} + I_{GPe} + I_{app}, \\ C_m \frac{dv_{TH}}{dt} &= -I_L - I_{Na} - I_K - I_T - I_{GPI} + I_{SM}(t). \end{aligned}$$

Here,  $C_m$  denotes the specific membrane capacitance of any given neuron.  $dv_R/dt$  represents the change in membrane voltage over time in a region  $R$ , and when multiplied with  $C_m$ , represents the current flowing through a neuronal membrane in region  $R$ .  $I_L, I_{Na}, I_K, I_T, I_{Ca}, I_{AHP}, I_{GPe}, I_{app}, I_{DBS}(t), I_{STN}, I_{GPI}, I_{SM}(t)$

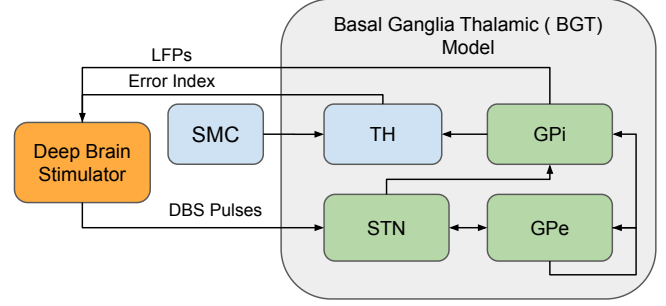


Figure 2: The Basal Ganglia-Thalamic Model

$I_T, I_{Ca}$ , and  $I_{AHP}$  denote the leak, sodium, potassium, low-threshold calcium, high-threshold calcium, and after hypo-polarization potassium channel currents, respectively. Variables of the form  $I_R$ , where  $R \in \{GPI, GPe, STN, TH\}$ , represent current flowing in from neurons in region  $R$ .

$I_{app}$  represents the external currents influential to the BG regions. Decreasing the contribution of  $I_{app}$  correlates with an insufficient dopamine supply from the substantia nigra pars compacta to the globus pallidus regions. This, in turn, leads to an increase in PD severity, as PD-afflicted neurons typically receive insufficient amounts of dopamine.  $I_{SM}(t)$  denotes the current contributed by the sensorimotor cortex (SMC) region to the TH. SMC contribution is modeled as an array of anodal monophasic current pulses of amplitude  $3.5 \mu A/cm^2$  and pulse width of 5 ms. The frequency at which these pulses occur is randomized via selecting from a gamma distribution with an average of 14 Hz and a coefficient of variation = 0.2.

Electrical stimulations are provided by our MAB algorithm to the BGT simulation via the  $I_{DBS}$  variable. We stimulate the STN region of the BG, a common target of most modern day DBS implementations. Applying these electrical impulses to the STN is known to lower symptom severity in PD patients and correct neural misfirings [1].

Now, we describe the Quality of Control (QoC) metrics which we consider for measuring the effect of DBS on the brain:

- (1) **Error Index (EI):** The EI captures the amount of erroneous activations that occur in the TH region of the brain with respect to the input pulses from the SMC. In a healthy brain, impulses from the SMC activate all the neurons in the TH exactly once in an interval of 25 ms. This is, however, not the case in a PD brain. Unfortunately, the EI is not possible to obtain in real life with the current devices in use for DBS.
- (2) **Beta-band Power Spectral Density ( $P_\beta$ ):** The GPI region of a PD brain exhibits pathological oscillations in the range of 13 – 35 Hz band (known as the beta-band) which is less prevalent in a healthy brain.  $P_\beta$  for a single neuron is given by  $P_\beta^j(x) = \int_{2\pi \cdot 13Hz}^{2\pi \cdot 35Hz} |\hat{f}(x_i)| df$ . The  $P_\beta$  of the entire region of the GPI neurons is calculated as  $P_\beta = \frac{1}{n} \sum_{j=1}^n P_\beta^j$ . The  $P_\beta$  value can be obtained in the real world from LFPs and is strongly correlated with the EI, therefore we use the  $P_\beta$  as feedback in our approach. A lower  $P_\beta$  reading is correlated with decreased PD symptoms in the patient.

### 3.2 Reinforcement Learning Algorithms for DBS

A variety of RL algorithms have been explored for DBS devices in literature, with deep-RL algorithms receiving more attention than the other RL approaches. Our work, however, focuses on the lightweight MAB algorithms for RL that make algorithms more suitable for DBS implants. First, this section elaborates on the deep-RL algorithms that have been widely studied in recent work and then describes the MAB algorithms we use in this paper.

In the context of DBS, the RL controller operates on the current neural state of the patient, represented as a vector of electrophysiological biomarkers. Formally, let the brain state at time step  $t$  be denoted by  $s_t = [b_1(t), b_2(t), \dots, b_n(t)] \in \mathcal{S}$ , where each  $b_i(t)$  corresponds to a biomarker for DBS. The RL agent observes  $s_t$  and selects a stimulation action  $a_t = [f_t, A_t] \in \mathcal{A}$ , where  $f_t$  and  $A_t$  represent the stimulation frequency and amplitude, respectively. The environment

(i.e., the patient's brain) responds to the stimulation with a new state  $s_{t+1}$ , and a scalar reward  $r_t$  reflecting therapeutic efficacy. The objective of the RL controller is to learn a policy  $\pi^*(a_t | s_t) = \arg \max_{\pi} \mathbb{E} [\sum_{t=0}^T r_t]$ , that maximizes the expected cumulative therapeutic reward while maintaining stability in the patient's neural dynamics. This control objective differs fundamentally from conventional RL applications, e.g., in games, where the agent aims to *continuously manipulate* the environment to achieve a dynamically shifting goal state. Instead, in DBS, the aim is to *identify and sustain* an optimal stimulation configuration  $(f^*, A^*)$  such that the  $P_{\beta}$  is minimized, i.e.,  $(f^*, A^*) = \arg \min_{(f, A) \in \mathcal{A}} P_{\beta}(s_{t+1})$ , thereby restoring and maintaining a stable, healthy brain state. The interaction of the BGT model with the RL agent is shown in Fig. 3.

**Deep Reinforcement Learning (Deep-RL):** Deep-RL algorithms combine reinforcement learning principles with deep neural networks to learn complex control policies directly from high-dimensional inputs. These algorithms aim to maximize cumulative reward by iteratively improving a policy that maps observations to actions, often through gradient-based optimization of a value or policy function. Among them, the Twin Delayed Deep Deterministic Policy Gradient (TD3) algorithm is a widely used actor-critic method designed to address overestimation bias in value learning. TD3 extends the Deep Deterministic Policy Gradient (DDPG) framework by employing two critic networks to compute a more reliable target value, delaying policy updates to stabilize learning, and adding noise to target actions for smoother value estimation. This enables TD3 to achieve robust and sample-efficient learning in continuous control tasks.

**Multi-Armed Bandit (MAB):** The Multi-Armed Bandit problem is a type of RL problem where a bandit learner must repeatedly choose between multiple actions with unknown rewards in an attempt to maximize cumulative rewards over time. Some of the popular MAB

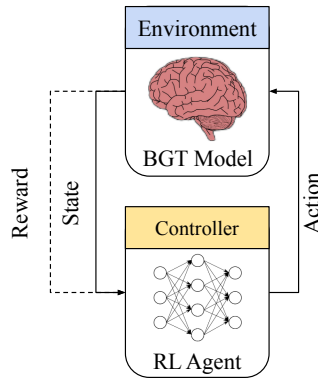


Figure 3: RL-BGT interaction.

algorithms that we use in the context of our paper for choosing stimulation parameters for DBS are as follows:

- (1) **Upper Confidence Bound (UCB):** This algorithm attempts to select actions based not only on their estimated rewards but also on the uncertainty (confidence interval) associated with those estimates. The action to be taken is determined using the following equation:

$$a_t = \arg \max_a \left[ Q(a) + c \cdot \sqrt{\frac{\log t}{n_a}} \right], \quad (1)$$

where  $t$  is the current timestep,  $n_a$  is the number of times the arm  $a$  has been played. The first term  $Q(a)$  denotes the action-value estimate of arm  $a$ , a higher value which is indicative of an arm which has received higher rewards. The second term takes into account the uncertainty (specifically, the upper confidence bound), which decreases as the arm is played more frequently. The constant  $c$  is a tuning parameter which scales the confidence interval. A larger value results in an increased likelihood of exploring actions with less certain rewards, whereas, a smaller value makes the algorithm inclined towards actions that seem to be more optimal based on the current knowledge. UCB naturally decays exploration over time.

- (2) **Thompson Sampling (TS):** Thompson Sampling uses a Bayesian approach to action selection. It maintains a probability distribution over each action's expected reward, capturing both the estimated value and the uncertainty in that estimate. At each timestep, a possible reward is sampled from this posterior distribution for every arm, and the arm with the highest sampled value is chosen. This method naturally balances exploration and exploitation, since actions with high uncertainty may occasionally yield large sampled rewards. The action selection rule is given by

$$a_t = \arg \max_a \tilde{\theta}_a, \quad \text{where } \tilde{\theta}_a \sim \mathcal{N}(\mu_a, \sigma_a^2).$$

Here,  $\tilde{\theta}_a$  is a random sample drawn from the posterior distribution of the expected reward for arm  $a$ , modeled as a Gaussian with mean  $\mu_a$  and variance  $\sigma_a^2$ . The parameters  $\mu_a$  and  $\sigma_a^2$  are updated based on the observed rewards and counts after each action. For more details, we direct the readers to [16].

- (3)  **$\epsilon$ -Greedy:** The  $\epsilon$ -greedy algorithm is a simple yet effective heuristic that balances exploration and exploitation by introducing randomness into the decision process. The algorithm chooses with probability  $\epsilon \in [0, 1]$ , an action uniformly at random (exploration), and with probability  $(1 - \epsilon)$ , selects the action with the highest estimated mean reward (exploitation). At each timestep  $t$ , the agent selects:

$$a_t = \begin{cases} \arg \max_a Q(a), & \text{with probability } 1 - \epsilon, \\ \text{random arm,} & \text{with probability } \epsilon. \end{cases} \quad (2)$$

Generally, the implementation of this algorithm involves starting with an initial  $\epsilon$  value and decaying the value of  $\epsilon$  by a certain factor until it reaches zero, after which only the arm with the highest estimated mean reward is used. This ensures that the algorithm converges to an optimal action.

(4) **Neural MAB:** The Neural MAB extends traditional bandits by using a neural network to approximate the reward function, allowing it to capture nonlinear relationships between context and reward. At each timestep  $t$ , the network estimates the expected reward  $Q(a, x_t)$  for each arm  $a$  and updates its parameters  $\theta$  based on the observed reward  $r_t$ . The action is selected as  $a_t = \arg \max_a f_\theta(x_t, a) + \eta_t$ , where  $f_\theta(\cdot)$  is the predicted reward and  $\eta_t$  is an exploration term. This approach enables generalization across arms and adapts effectively in complex or non-stationary environments, combining deep learning's expressiveness with classical bandit exploration.

## 4 Methodology

We begin by presenting our formulation of the MAB problem for selecting appropriate stimulation parameters in DBS. Next, we outline the reward function employed in our implementation. We then conclude the section with a description of our proposed algorithm.

### 4.1 Problem Formulation

The frequency and amplitude selection task is formalized as a sequential decision making problem under uncertainty, where the goal is to maximize therapeutic benefit while minimizing side effects. Specifically, we model each combination of candidate stimulation frequency  $f_p \in \mathcal{F}$  and amplitude  $a_q \in \mathcal{A}$  as an arm  $(f_p, a_q)$  in a MAB setting, where  $p \in \{1, 2, \dots, m\}$  and  $q \in \{1, 2, \dots, n\}$  index the  $m$  candidate frequencies and  $n$  candidate amplitudes respectively. Therefore, we derive a set of candidate actions  $\mathcal{X} = \{(f_i, a_j) \mid i = 1, \dots, m; j = 1, \dots, n\}$ ,  $|\mathcal{X}| = m \cdot n$ . At every decision point  $t$ , an arm  $(f_{p,t}, a_{p,t})$  is chosen and a reward is obtained based on the outcome which is then used by the MAB algorithm to learn how the arms compare in terms of effectiveness, which in our context is the overall positive outcome of the patient.

### 4.2 Reward Function

We describe the formulation of our reward function here. The playing of every arm follows an instantaneous reward. In our setup, the instantaneous reward after using an arm is given by  $R_{\text{instant}}(t) = \alpha \cdot r_1 + \beta \cdot r_2 + \gamma \cdot r_3$ , which is a function of the following components:

- (1) **PD Intensity** ( $r_1$ ): As mentioned earlier, a lower  $P_\beta$  is indicative of reduced PD symptoms. Thus, we calculate PD intensity from the  $P_\beta$  reading during the application of the arm and incorporate it into the reward function with  $r_1 = P_\beta$ .
- (2) **Continuous periods of no stimulation:** It has generally been considered safer to provide DBS with longer periods of no stimulation to the human brain, that is, with longer pulse intervals. The second component of our reward  $r_2$  is calculated as

$$r_2 = \begin{cases} 1, & \text{if } I_{\text{DBS}}[t] = 0 \\ 0, & \text{otherwise.} \end{cases} \quad (3)$$

Where  $I_{\text{DBS}}[t]$  is the amplitude of DBS current provided to the brain at time step  $t$ . Note that the duration of a single stimulation period in our implementation is 0.01 ms.

- (3) **Energy Consumption:** Since the device runs on a battery, we would like to conserve the battery life of the device to minimize the need for frequent charging and therefore surgeries

for battery replacements in the long run. Also, it is favorable for the health of the patient to provide only as much stimulation to the brain as necessary for their well-being. Therefore, we incorporate energy consumption into our reward, calculated as

$$r_3 = I_{\text{RMS}} = \sqrt{\frac{1}{T} \int_0^T I_{\text{DBS}}^2(t) dt}, \quad (4)$$

where  $T$  is the total duration of  $I_{\text{DBS}}$  of the STN region.

Note that all the components of the reward function are scaled to the range  $[0, 1]$  to ensure stability of the algorithm. The coefficients  $\alpha, \beta$  and  $\gamma$  used are  $-0.7, 0.1$  and  $-0.2$ , respectively.

### 4.3 Proposed Approach: T3P Bandit

In our experiments, a few of the existing MAB algorithms have demonstrated the ability to converge to optimal stimulation parameters with the right choice of parameters in a reasonable time frame. However, as with many RL frameworks, such algorithms can be further improved by adapting to the unique characteristics of their target domains. Through our experiments, we observe that the mean reward obtained from each arm can be sufficiently estimated by playing all the arms just once. Furthermore, we find that arms among these which returned below-average rewards never turned out to be the optimal arm and were always ones that are unsuitable for DBS in the current state. We use this domain knowledge to add a pruning technique to the well-known  $\epsilon$ -greedy bandit algorithm to create our Time & Threshold-Triggered Pruned (T3P) MAB algorithm. Our modification to the existing algorithm restricts its exploration to a set of arms which are good candidates for the stimulation parameters thus reducing instances of stimulation using non-optimal arms during exploration while also leading to faster convergence.

The working of our T3P MAB agent is given in Algorithm 1. The algorithm starts with a warm-up phase where it plays all arms once to get an estimate of the associated rewards. The  $\epsilon$  parameter does not start decaying until the warm-up phase is complete. At the end of the warm-up phase, all arms except the top  $K$  are pruned, with the bandit only able to choose from the top  $K$ . At every round, an arm  $i$  is played and the LFPs from the GPi region is recorded consequently. The  $P_\beta$  is calculated from these recorded LFPs as given in Section 3 and it is used to compute the reward for that arm along with characteristics of the DBS current as discussed earlier in Section 4.2. This reward is used to update the value estimate  $Q_i$  of the arm  $i$ . A higher  $Q$  value indicates a more effective arm.

With the decaying of  $\epsilon$ , the algorithm converges to the optimal arm. Given that the T3P bandit has a high convergence rate, it is triggered again once a countdown timer elapses. This is done in order to update the DBS signal to adapt to the brain state in case it has changed but is not observable through the biomarker. The other scenario when it is triggered is when a change in the state of the brain (through the  $P_\beta$  biomarker) is observed. This might be detected by a deviation from the reading of the  $P_\beta$  biomarker by a certain threshold, in which case, the T3P algorithm will be triggered again in an attempt to find the new optimal arm. The parameter  $K$  is tunable. Details on tuning this parameter is discussed later in Section 5.2. Subsequently, we compare our proposed algorithm against other existing MAB approaches for DBS in Section 5.3.

**Algorithm 1:** T3P MAB for DBS Parameters Selection

---

**Input** :Number of arms  $A$ , decay parameters  $(\epsilon_{start}, \epsilon_{min}, decay\_steps)$ , top- $K$  arms  $K$ , biomarker  $P_\beta$ , deviation threshold  $\delta$

**Output**:Optimal arm  $a^*$  for stimulation

**procedure** T3P( $A, \epsilon_{start}, \epsilon_{min}, decay\_steps, K, P_\beta, \delta$ )

- // Warm-up Phase: Play all arms once
- for  $a = 1$  to  $A$  do
  - Play arm  $a$ , observe reward  $r_a$
  - Update estimated reward  $Q(a)$  and count  $n(a)$
- // Prune arms: keep only top  $K$  based on rewards
- Sort all arms by  $Q(a)$  in descending order
- Keep only top  $K$  arms, discard the rest
- // Start epsilon decay only after warm-up
- $\epsilon \leftarrow \epsilon_{start}$
- $t \leftarrow 0$
- while** True **do**
  - $t \leftarrow t + 1$
  - //  $\epsilon$ -greedy selection among top  $K$  arms
  - Generate  $u \sim U(0, 1)$
  - if**  $u < \epsilon$  **then**
    - Select a random arm  $a_t$  from top- $K$
  - else**
    - $a_t \leftarrow \arg \max_{a \in K} Q(a)$
  - Play arm  $a_t$ , observe reward  $r_t$
  - Update  $Q(a_t)$  and  $n(a_t)$  based on  $r_t$
  - // Decay epsilon
  - $\epsilon \leftarrow \max(\epsilon_{min}, \epsilon_{start} - \delta \cdot t)$
- return**  $a^* = \arg \max_{a \in K} Q(a)$

---

The work most closely related to ours is a recent study that employs a modification of the neural TS MAB algorithm to tune only the frequency of stimulations [12]. With our best implementation of this method, it frequently converges to a suboptimal arm. In instances where it does reach the optimal arm, it uses non-optimal parameter settings for prolonged time periods which could result in an unfavorable experience for the patient.

## 5 Experimental Results

Next, we discuss the results with the T3P MAB algorithm while comparing it with other MAB approaches as well as existing deep-RL approaches for DBS in terms of efficiency in suppressing PD symptoms. We then discuss in detail our implementation on hardware and report power measurements. Finally, we compare these power measurements with existing approaches. This proves the effectiveness of our approach in terms of not only performance but also energy efficiency.

### 5.1 Experimental Setup

As mentioned earlier, we perform the experiments on the computational BGT model from [13]. We use frequencies in the range [55, 180] Hz as frequencies lower than 50 Hz have shown to be ineffective for

DBS. Amplitudes that the algorithm could use were restricted to the range [0, 5000]  $\mu A/cm^2$ . Works regularly implement DBS with these set ranges and have found them safe for *in-vivo* use [4, 5]. Our MAB algorithm attempts to choose from 31 arms which are combinations of candidate frequency values {55, 80, 105, 130, 155, 180} Hz and candidate amplitude values {0, 1000, 2000, 3000, 4000, 5000}  $\mu A/cm^2$ . The pulse duration used for DBS is 300  $\mu s$ . We use a bi-phasic current for charge balancing in the brain. Charge balancing is necessary as it lowers the risk of negative faradic reactions with brain tissue [21]. The DBS waveform is therefore symmetric where an anodic current for 150  $\mu s$  is followed by a cathodic current for 150  $\mu s$ . The length of each round in our implementation is 1000 ms.

With the setup described above, we analyze the performance of our algorithm on the following hardware platforms:

- (1) The **ESP32-S3** uses a processor with dimensions 5 mm x 5 mm and is suitable for a device that needs to be implanted inside the human body. The device uses a dual-core Xtensa LX7 CPU with a maximum CPU frequency of 240 MHz, and contains 512 kB SRAM and 384 kB ROM. It further supports Wi-Fi and Bluetooth connectivity for communication with external devices to monitor health metrics of the patient. The system operates at a nominal voltage of 3.3 V, consistent with standard low-power embedded platforms.
- (2) The **ESP32-P4** which comes with a dual-core RISC-V CPU that runs up to 400 MHz, 768 kB SRAM and a low power core that can run at 40 MHz. This MCU too comes in a size that can be used for implantable devices with the dimensions of the processor being 10 mm x 10 mm.

To accurately measure the power consumption of these MCUs during operation, we use the **Joulescope JS220** Precision Energy Analyzer. The JS220 enables high-resolution, real-time measurement of various power consumption metrics, allowing precise computation of instantaneous power and total energy consumption over time. Data was recorded using the Joulescope software interface to capture detailed energy profiles of the ESP32 MCUs under various DBS algorithms.

### 5.2 Hyper-parameter Tuning of the T3P MAB algorithm

We will now discuss how we tune the hyperparameters of the T3P MAB algorithm, namely the exploration rate ( $\epsilon$ ) and the number of top arms  $K$  considered for DBS after the warmup phase. As discussed in section Section 4.3, the T3P MAB algorithm prunes arms which are less likely to be effective for DBS in order to reduce the search space of the MAB algorithm. As usual,  $\epsilon$  is the exploration probability. We perform a grid search for finding the optimal combination of  $\epsilon$  and  $K$ . It can be seen from Fig. 4 that the highest cumulative average reward is obtained by a combination of  $\epsilon = 0.2$  and  $K = 25$ . The average cumulative rewards calculation is based on 10 runs of the T3P MAB algorithm for each  $\epsilon$  and  $K$  combination. A higher average reward value is marked with a greener value with lower values marked in red. We experiment with  $K$  values in the range [5, 30] as we have 31 arms in total. A  $K$  value of 30 means that only one arm is pruned at the end of the warmup stage and the algorithm can explore from a total of 30 arms after that. The heatmap shows the trend of a lower  $\epsilon$  being able to accumulate more rewards. This is because a higher

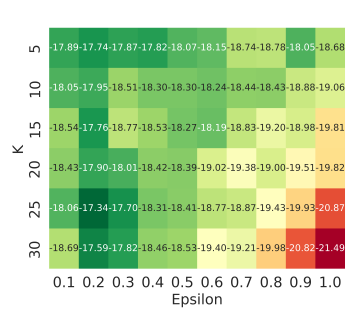


**Figure 4: Hyper-parameter tuning of T3P MAB using cumulative rewards.**

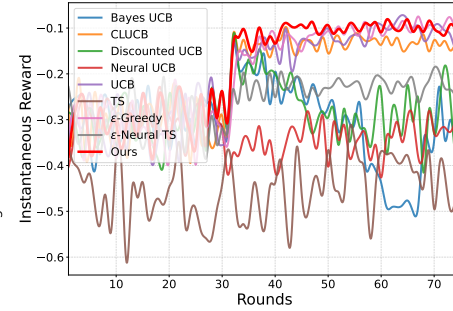


**Figure 5: Comparison of MAB algorithms based on instantaneous rewards over time.**

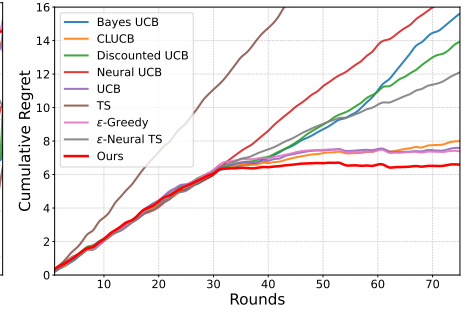


**Figure 6: Comparison of MAB algorithms based on cumulative regret over time.**

exploration probability may result in playing more non-optimal arms unnecessarily. However, this trend is broken at  $\epsilon = 0.1$  because extremely low exploration can result in convergence to a non-optimal arm. The choice of top K restricts the exploration space. For higher exploration probabilities, a lower value of K can be seen to gather more rewards although this is less prominent for  $\epsilon$  values under 0.4. For our implementation, we linearly decay  $\epsilon$  by 0.025 after each episode.

### 5.3 Comparison with other MAB approaches

We compare our proposed T3P agent against 8 other MAB algorithms, namely Upper Confidence Bound (UCB), Bayes UCB [14], Discounted UCB [11], Neural UCB [33], CLUCB [15], Thompson Sampling (TS),  $\epsilon$ -Greedy and the  $\epsilon$ -Neural Thompson Sampling technique in [12]. Note that  $\epsilon$ -Neural Thompson sampling was proposed for a setting where only the frequency of the DBS current could be modulated. We modify its implementation for our experiments to allow it to change both frequency and amplitude of the stimulations. The results of these algorithms are based on their best hyper-parameter settings. We use  $c = 0.05$  for UCB,  $c = 1.0$  for Bayes UCB,  $c = 0.6$  and  $\alpha = 0.05$  for CLUCB,  $c = 0.35$  and  $\gamma = 0.99$  for Discounted UCB,  $\alpha = 0.9$  and  $\lambda = 0.75$  for Neural UCB,  $\epsilon = 0.4$  for  $\epsilon$ -Greedy,  $\epsilon = 0.1$  for  $\epsilon$ -Neural TS.

The comparison of their performance in terms of average instantaneous rewards obtained over 75 rounds is shown in Fig. 5. The values on the x-axis are the average instantaneous rewards based on 10 runs for each algorithm. The instant reward is derived from the proposed reward function that also serves as feedback to the algorithms. As shown in the graph, the T3P MAB algorithm exhibits the fastest convergence toward the optimal arm and consistently outperforms other algorithms in terms of instantaneous rewards and convergence speed.  $\epsilon$ -Greedy, UCB and CLUCB, although worse than T3P, were close to each other with regard to the same metrics. The  $\epsilon$ -Neural TS often converged to a suboptimal arm. However, the other MAB algorithms failed to converge by the end of 75 rounds.

The cumulative regret of each of these algorithms over time based on the average of 10 runs of the algorithms is shown in Fig. 6. Instantaneous regret at time  $t$  is calculated as the difference between the reward obtained by the optimal arm, if it was played in that round, and the reward obtained by the arm the MAB algorithm actually played at time  $t$ . The UCB, Epsilon-Greedy and our proposed T3P

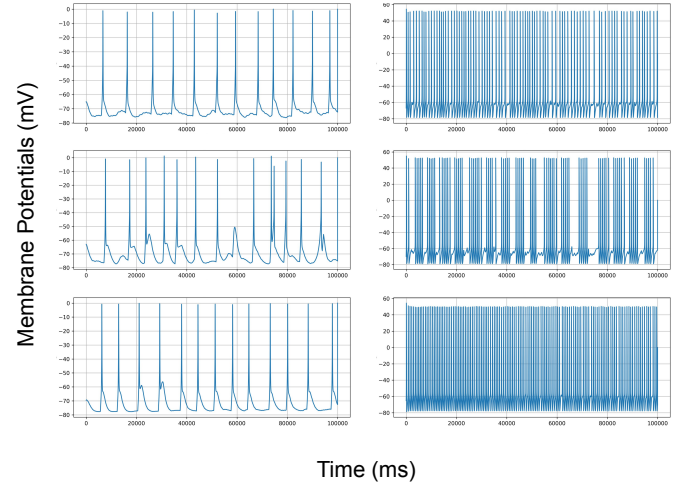


**Figure 7: Neuron activity in the TH (left) and GPi (right) in a healthy brain (top row), a PD brain (middle row) and a PD brain with DBS (bottom row)**

MAB algorithms all converge to the optimal arm, with the T3P algorithm converging more quickly than the others. The other MAB algorithms failed to converge to the optimal arm in almost all cases. The optimal arm chosen for regret calculation was the one that used a frequency of 155 Hz and an amplitude of  $1000 \mu\text{A}/\text{cm}^2$  based on empirical observations.

We observe that *neural* variations of MAB algorithms, in general, fail to perform as well as the other MAB algorithms. We believe this is due to the fact that it involves training a neural network to estimate the rewards from actions. Neural network components, being sample inefficient, require more rounds to converge. Also, the possibility of a change in state of the brain is not considered in [12] in which case, the neural network would have to be trained from scratch again. In Fig. 7, the activity of the membrane potentials in a single neuron is shown from our simulation of a healthy and a PD brain. The figure also shows how the activity in a PD brain changes when DBS is enabled with the T3P MAB agent. The characteristics of a PD brain, which are missed spikes in neurons in the TH region and occurrence of spikes in bursts in the GPi region are shown in the left and right

| Condition/Setup       | $P_\beta V_{Gi}$<br>( $\mu V^2 Hz^{-1}$ ) | Power Usage<br>( $\mu A cm^{-2} Hz$ ) |
|-----------------------|---|---------------------------------------|
| Healthy               | 348000                                    | –                                     |
| PD                    | 896000                                    | –                                     |
| o-DBS [4]             | 361000                                    | 492                                   |
| TD3 Deep-RL [4]       | 336000                                    | 341                                   |
| <b>T3P MAB (ours)</b> | <b>189951</b>                             | <b>216</b>                            |

**Table 1: Comparison with existing approaches for DBS**

figure in the middle row respectively. In the figures shown in the last row, both these characteristic features vanish with DBS applied to the brain. Fig. 8 shows the  $P_\beta$  reduction with the T3P agent after it has converged. It can be noticed that the  $P_\beta$  never crosses the value from that of a normal brain which is indicative of the fact that the patient symptoms are suppressed.

#### 5.4 Comparison with existing deep-RL methods

We use the implementation of the Twin-Delayed Deep Deterministic Policy Gradient (TD3) agent [4], which is the state-of-the-art in DBS for PD among other deep RL algorithms and establish that the more computationally efficient MAB algorithms show performance comparable to deep RL methods in terms of suppressing the  $P_\beta$  biomarker and energy used for generating DBS signals.

However, it should be noted that the technique used for  $P_\beta$  computation in their work is different than how we do it for the experiments. The  $P_\beta$  calculation for the TD3 agent was done by computing the  $P_\beta$ s of individual neurons from membrane potential readings (accessible from the computational BGT model) and averaging them to find the  $P_\beta$  which they report in their results. In our experiments, we compute the mean of the membrane potentials of the 10 neurons to get the LFP which is then used to compute  $P_\beta$ . The technique we use can be considered more realistic as the former technique requires precise sensors (in order to extract membrane potential readings from singular neurons) which are more expensive and uncommon for DBS implants. LFPs, which are recordings of membrane potentials from a group of neurons, are simpler to obtain and commonly used in practice so we use this method to compute the  $P_\beta$  biomarker. In order to compare between the techniques, however, we resort to the former method for computing the biomarker.

In Table 1 we compare the the energy consumption for stimulation in addition to patient outcome from an open-loop DBS (o-DBS), the TD3 deep-RL algorithm and our proposed T3P MAB. For the results, the initial exploration stage of the T3P MAB algorithm before the algorithm converges to an arm is not considered. Similarly, for the TD3 agent, we do not report values from the training phase but after it has been deployed for DBS. The comparison of patient outcomes is done in terms of  $P_\beta$  of the  $V_{Gi}$  signal from the BGT model. The power comparison is done as per the formula in Eq. (4). The results for the o-DBS setup and the TD3 Deep-RL are taken from [4]. For the o-DBS, a constant frequency of 130 Hz and an amplitude of  $2500 \mu A/cm^2$  is considered which is typical value used for most patients. The TD3 agent was trained on episodes of length 1000 ms with a timestep of 100 ms which allowed the upation of the stimulation parameters 10 times during each episode. It was trained for a maximum duration of 5000 timesteps or until the rewards converged. It uses a state

representation consisting of the standard deviation of the synaptic conductance of the GPi neurons  $S_{Gi}$ , the Hjorth parameters (which include the activity, mobility and complexity) of the  $S_{Gi}$  signal,  $P_\beta$  of the GPi neurons and sample entropy, which is a measure of self-similarity of neuron readings of the STN. The reward function for the TD3 agent takes into account the energy consumption and the power spectral density (PSD) of the  $S_{Gi}$  signal in the range 1 – 20 Hz which is also a biomarker that is correlated with PD symptoms in a patient. We however we observe only the widely accepted  $P_\beta$  from the GPi region for our reward function as discussed in Section 3.

From Table 1, we can see that our MAB approach consumes less power while also being able to suppress the  $P_\beta$  value better than the o-DBS and TD3 Deep-RL approaches. The RL agent was reported to use an average frequency and amplitude of 135 Hz and  $1690 \mu A/cm^2$  respectively. We found our approach to converge to the arm using a frequency of 155 Hz and  $1000 \mu A/cm^2$  in almost all cases. Additionally, it was observed that this combination always received more rewards on average than the other candidate parameter settings we consider for DBS.

The TD3 agent relies on the PSD computation of the membrane potentials of the GPi neurons  $V_{Gi}$  and  $S_{Gi}$  signals sampled for a duration of 100 ms. Through our experiments, we find that a duration of 100 ms might not be long enough to obtain an accurate estimate of the PSD of a signal. Calculation of PSD based on signal lengths shorter than 500 ms were found to be too unreliable for distinguishing between a more effective arm from a less effective one in the BGT model. This could also be an explanation of why the RL agent converged to a non-optimal frequency and amplitude setting as our approach beats the TD3 agent in both the aspects that were considered in its reward function – power usage and alleviation of patient symptoms (quantified by the  $P_\beta$  reading). Note that we, in contrast, use a round length of 1000 ms. Other possible reasons could be the unsuitability of the parameters used for state representation. A feature which is loosely correlated with patient outcome or associated with a lot of noise can stunt the ability of a deep-RL algorithm to learn the optimal policy. It is also worth noting that increasing the timestep length of an RL algorithm can lead to the requirement of a longer training time and/or more training data both of which can be difficult to achieve in practice.

An additional advantage of using MAB algorithms is the ability to quickly adapt to a case where the user is facing an unexpected side effect or discomfort with the specific parameter setting the algorithm has converged to. An example of this is shown in Fig. 9 where the user intervenes at round 75. By the end of round 111, it can be seen that the algorithm has converged to the second optimal arm, now that the optimal one has been pruned. This is however not straightforward with deep-RL techniques as the neural network component maps a state to an action and it would be difficult to choose an alternative action if the action returned is not acceptable for the patient.

#### 5.5 Implementation on Hardware

As described in detail in Section 5.1, we implement our proposed T3P MAB algorithm on the ESP32-P4 and ESP32-S3 MCUs and measure energy metrics using the Joulescope. For each round,  $V_{Gi}$  signals are sampled at a rate of 100 kHz, which is the highest rate permitted by the BGT model. Our BGT model plays an arm with the stimulation

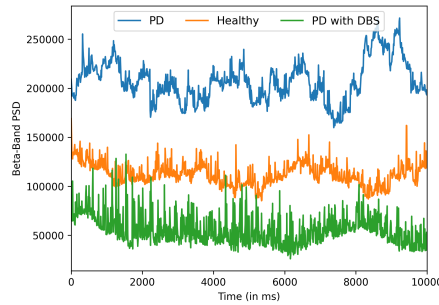


**Figure 8:  $P_\beta$  suppression with DBS from T3P MAB.**

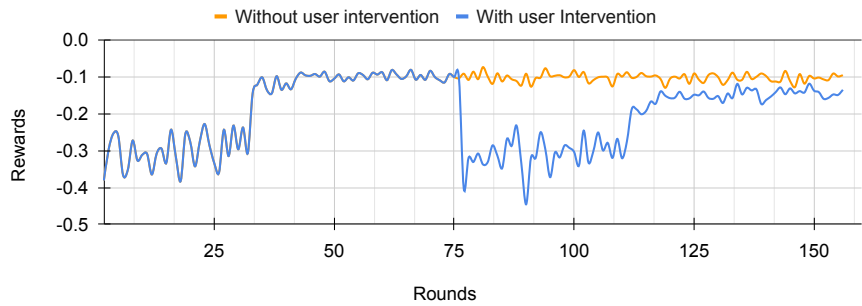


**Figure 9: Illustration of the adaptability of the T3P algorithm when a patient intervention is introduced due to reported discomfort.**

| MCU      | Clock Rate (MHz) | Algorithm | Round Length (s) | Current Draw (mA) | Voltage (V) | Power Consumption (mW) | Energy Usage (J) | Time to Converge (s) |
|----------|------------------|-----------|------------------|-------------------|-------------|------------------------|------------------|----------------------|
| ESP32-S3 | 240              | T3P MAB   | 1.2              | 37.7              | 5.13        | 183.5                  | 5.4              | 46.8                 |
|          |                  | T3P MAB*  | —                | 31.6              | 5.13        | 162.4                  | 4.8              | —                    |
| ESP32-S3 | 160              | T3P MAB   | 1.3              | 32.0              | 5.13        | 164.1                  | 4.9              | 50.7                 |
|          |                  | T3P MAB*  | —                | 28.5              | 5.13        | 146.3                  | 4.3              | —                    |
| ESP32-S3 | 80               | T3P MAB   | 1.7              | 27.6              | 5.13        | 141.5                  | 4.2              | 66.3                 |
|          |                  | T3P MAB*  | —                | 24.8              | 5.13        | 127.2                  | 3.8              | —                    |
| ESP32-S3 | 40               | T3P MAB   | 2.4              | 17.8              | 5.13        | 91.9                   | 2.7              | 93.6                 |
|          |                  | T3P MAB*  | —                | 16.1              | 5.13        | 82.2                   | 2.4              | —                    |
| ESP32-P4 | 360, 360         | T3P MAB   | 1.1              | 68.5              | 5.12        | 352.1                  | 10.4             | 42.9                 |
|          |                  | T3P MAB*  | —                | 67.3              | 5.12        | 344.7                  | 10.2             | —                    |
| ESP32-P4 | 180, 180         | T3P MAB   | 1.2              | 64.4              | 5.12        | 329.7                  | 9.8              | 46.8                 |
|          |                  | T3P MAB*  | —                | 63.2              | 5.12        | 323.4                  | 9.6              | —                    |
| ESP32-P4 | 90, 90           | T3P MAB   | 1.4              | 58.9              | 5.12        | 302.1                  | 9.0              | 54.6                 |
|          |                  | T3P MAB*  | —                | 57.2              | 5.12        | 293.2                  | 8.7              | —                    |
| ESP32-P4 | 40, 40           | T3P MAB   | 1.9              | 55.2              | 5.12        | 282.7                  | 8.4              | 74.1                 |
|          |                  | T3P MAB*  | —                | 54.4              | 5.12        | 278.5                  | 8.3              | —                    |

\* Indicates readings after the T3P MAB has converged to an arm

**Table 2: Measurements with different clock frequencies on different MCUs**

parameters decided by the algorithm while recording the  $V_{Gi}$  signals for 1000 ms second. At the end of the round, the  $P_\beta$  from the  $V_{Gi}$  signal is calculated and is used to update the parameters of the MAB algorithm.

We found the  $P_\beta$  calculation to be the most resource intensive step of the algorithm. This is because every time we want to find the  $P_\beta$  after a round, we have a total of 100,000 float values to be processed. However, in order to perform an FFT over all the samples they would need to be loaded onto the RAM at the same time which is not feasible. Therefore, we break down the signal into chunks and process them separately to

compute the FFT and thereafter the  $P_\beta$ . Specifically, we used a Radix-2 Cooley–Tukey Decimation-in-Time (DIT) algorithm, which efficiently computes the discrete Fourier transform by recursively decomposing the input signal into even and odd indexed components and combining the partial results using precomputed twiddle factors. This in-place, iterative implementation minimizes both computational overhead and memory usage, making it well-suited for deployment on embedded hardware such as the ESP32 platform.

Now that we have discussed the details of our implementation on the MCU we will now describe the statistics we observe from the JoulescopeJS220 after deployment on the hardware. Table 2 enlists observations from the MCUs with different clock speeds. For each of the cases, we record the time per episode, convergence time of the algorithm, current draw, voltage, power consumption and their time



**Figure 10: ESP32-S3 MCU used for our T3P MAB.**

to converge to an arm for running our proposed algorithm. These energy measurements are based on a window of 30 s. We experiment with 4 different clock frequencies for both the MCUs – 240, 160, 80 and 40 with the ESP32-S3, and 360, 180, 90 and 40 with both cores in the ESP32-P4. The third low-power core on the ESP32-P4 was disabled for all experiments.

It can be observed from the table that the power consumption increases with an increase in the clock frequency as expected. The power draw, voltage and energy readings are the average values recorded over 30 seconds. For every MCU and frequency, the measurements from the T3P MAB agent is recorded. The first reading in every row records the measurements from when the T3P algorithm is running and the second readings are from when the MAB algorithm has converged and is using a fixed stimulation parameter. A trade-off can be noticed here – a setup that consumes less power is associated with longer convergence time. However, in all of these cases the algorithm takes less than two minutes to converge which is clinically acceptable for patient use.

It is to be noted that it was not possible for the TD3 deep-RL algorithm to be trained on the MCUs we consider for experiments. Although [4] talks about the possibility of *in vivo* training in human brains, deep-RL algorithms take hours to train on traditional GPUs and would take even longer on MCUs given their limited computational capabilities. Hence, the goal of enabling personalized medicine by the deep-RL agent to be trained *in vivo* has not been realized in the work.

Without the ability to train deep-RL agents inside the implant, they are traditionally trained offline and only deployed after their rewards have converged. This offline training process involves collecting patient data while using different stimulation parameters to create a dataset. This dataset is then used to train the RL agent before deploying it on the implant. This dataset is also prone to being outdated with changes in the patient's brain over time (possibly with neurodegenerative progression) and might need training of the RL agent all over again in the future. Our MAB approach, on the other hand, does not suffer from this limitation. This because of the fact that it does not freeze parameters but rather tries to find the optimal arm based on the new distribution of rewards in the current state of the brain.

The MAB is expected to still remain more energy efficient even when the TD3 deep-RL agent is deployed on the MCU post training, due to the fact that it is able to avoid the requirement of inferencing a neural network every 100 ms. Also, our T3P MAB algorithm relies only on the  $P_\beta$  reading from the GPi neurons in contrast to the 6 features required by the TD3 agent for state representation, one of which requires an FFT to be performed, which clearly makes it more compute intensive than our T3P MAB agent.

## 5.6 Comparison with Existing Hardware

Finally, we would like to compare our most energy-efficient hardware implementation against DBS devices that have already been used in clinical trials. Existing devices for DBS are enlisted in Table 3, namely Neurochip-2 [31], PennBMBI [18], Toronto [3, 24, 25], Activa P+S [2, 17, 27, 30], WAND [32], Summit RC+S [28] and our T3P agent deployed on the ESP32-S3 with a clock rate of 40 MHz, along with their power consumption, maximum current for DBS, sampling rate

and their closed-loop policy. It can be seen that our setup beats three out of the six other setups in terms of power consumption. Our choice of maximum current is at par with most of these devices except the most recent Summit RC+S which uses a maximum stimulation current of 25.5 mA. It is noteworthy that most other devices that use a lower sampling rate also consume less power than our implementation. This is likely due to the fact that processing more samples, especially performing FFTs, can be compute intensive. It could therefore be worthwhile to attempt to decrease the sampling rate to estimate the biomarker. This is, however, beyond the scope of this work.

Although some of these commercial DBS devices demonstrate excellent power efficiency, they still rely on policies using thresholds or SVMs. These approaches typically require a calibration phase, to collecting patient-specific data and tuning model parameters offline, which can impose additional burden on patients. Moreover, as explained before, neural activity and biomarker characteristics may evolve over time, the parameters determined during initial calibration may gradually lose optimality, potentially degrading long-term performance. Therefore, the use of RL methods in our work is a step towards precision medicine, where the implant adapts with the current state of the brain and progression of PD, rather than relying on outdated patient data. Most of these devices are also implemented on custom-designed MCUs, enabling careful optimization of hardware resources to minimize current leakage and overall power consumption. Exploring such customized hardware co-design remains an important direction for future work.

## 6 Concluding Remarks

In this work, we presented a resource-conscious, adaptive framework for Deep Brain Stimulation (DBS) using lightweight reinforcement learning (RL) methods rooted in Multi-Armed Bandit (MAB) theory. We developed the Threshold-Triggered and Pruned (T3P) MAB algorithm and therefore demonstrated that clinically relevant DBS control can be achieved by significantly lower computational complexity, faster convergence, and higher energy efficiency compared to traditional deep reinforcement learning (deep-RL) approaches such as TD3. Our formulation unifies frequency and amplitude tuning within a single decision space, a capability that remains largely unexplored in prior DBS literature. By simultaneously optimizing both parameters based on neurophysiological biomarkers, the proposed method improves adaptability and patient safety while meeting the stringent hardware and energy constraints of implantable systems.

Our T3P MAB algorithm improves upon the conventional  $\epsilon$ -greedy approach by considering domain-specific characteristics. This mechanism enables rapid convergence while maintaining responsiveness to changes in the patient's brain state. Our results showed that the algorithm can identify optimal stimulation parameters more quickly than existing MAB approaches. Moreover, it beats existing deep-RL approaches in suppressing the  $P_\beta$  biomarker while utilizing less power. Importantly, the algorithm is also capable of robust adaptability to user intervention where a patient experiences discomfort.

To our knowledge, this is the first hardware implementation of an MAB-based DBS controller that includes quantitative power and energy measurements on modern microcontrollers. In contrast, the TD3 deep-RL agent could not be feasibly trained or executed on such hardware due to its memory and computation requirements,

| Attributes                | Neurochip-2                       | PennBMBI                          | Toronto   | Activa P+S | WAND      | Summit RC+S                | Ours    |
|---------------------------|-----------------------------------|-----------------------------------|-----------|------------|-----------|----------------------------|---------|
| <b>Power</b>              | 284 – 420 mW                      | 290 mW                            | 45 mW     | 500 uW     | 172 mW    | 2.5 mW                     | 82.2 mW |
| <b>Max. Current</b>       | 5 mA                              | 1 mA                              | 3 mA      | 25.5 mA    | 5 mA      | 25.5 mA                    | 5 mA    |
| <b>Sampling Rate</b>      | 2/24 kS/s                         | 21 kS/s                           | 15 kS/s   | 422 S/s    | 1 kS/s    | 1 kS/s                     | 10 kS/s |
| <b>Closed-loop Policy</b> | Detection/<br>threshold-triggered | Detection/<br>threshold-triggered | Threshold | 2D SVM     | Threshold | 8D SVM,<br>RL<br>Threshold | (MAB)   |

Table 3: Comparison with measurements from existing devices for Deep Brain Stimulation [28].

highlighting the suitability of bandit-based methods for implantable devices. Future work will explore the possibility of further reducing convergence time of the algorithm, implementation of the closed-loop setup in hardware and experiments with real patient data.

In conclusion, this paper demonstrates that adaptive, resource-efficient neuromodulation using RL is both feasible and effective. Our T3P MAB algorithm delivers performance comparable to state-of-the-art deep-RL controllers at a fraction of their energy cost and computational demand. By aligning algorithmic efficiency with hardware constraints, our work is a step toward energy-aware intelligent DBS systems. Our approach further enables patient-specific adaptation without the need for prior training in real-world clinical settings.

## References

- [1] Elie M Adam et al. 2021. Deep brain stimulation in the subthalamic nucleus for Parkinson's disease can restore dynamics of striatal networks. *bioRxiv* (2021). arXiv:<https://www.biorxiv.org/content/early/2021/08/29/2021.08.29.458121.full.pdf> doi:10.1101/2021.08.29.458121
- [2] Al-Thaddeus Avestruz et al. 2009. A 5 W/Channel Spectral Analysis IC for Chronic Bidirectional Brain–Machine Interfaces. *Solid-State Circuits, IEEE Journal of* 43 (01 2009), 3006 – 3024. doi:10.1109/JSSC.2008.2006460
- [3] Arezzi Bagheri et al. 2013. Massively-Parallel Neuromonitoring and Neurostimulation Rodent Headset With Nanotextured Flexible Microelectrodes. *IEEE Transactions on Biomedical Circuits and Systems* 7, 5 (Oct 2013), 601–609. doi:10.1109/TBCAS.2013.2281772
- [4] Nicholas Carter et al. 2025. In-Vivo Training for Deep Brain Stimulation. arXiv:2510.03643 [cs.LG] <https://arxiv.org/abs/2510.03643>
- [5] Chia-Hung Cho et al. 2024. Closed-Loop Deep Brain Stimulation With Reinforcement Learning and Neural Simulation. *IEEE Tran. Neural Systems & Rehabilitation Engg.* 32 (2024), 3615–3624. doi:10.1109/TNSRE.2024.3465243
- [6] John E. Fleming, Eleanor Dunn, and Madeleine M. Lowery. 2020. Simulation of Closed-Loop Deep Brain Stimulation Control Schemes for Suppression of Pathological Beta Oscillations in Parkinson's Disease. *Frontiers in Neuroscience* Volume 14 – 2020 (2020). doi:10.3389/fnins.2020.00166
- [7] Qitong Gao et al. 2020. Model-Based Design of Closed Loop Deep Brain Stimulation Controller using Reinforcement Learning. In *11th International Conference on Cyber-Physical Systems (ICCPs)*. doi:10.1109/ICCPs48487.2020.00018
- [8] Qitong Gao et al. 2022. Offline Policy Evaluation for Learning-based Deep Brain Stimulation Controllers. In *2022 ACM/IEEE 13th International Conference on Cyber-Physical Systems (ICCPs)*. 80–91. doi:10.1109/ICCPs54341.2022.00014
- [9] Qitong Gao et al. 2023. Offline Learning of Closed-Loop Deep Brain Stimulation Controllers for Parkinson Disease Treatment. In *Proceedings of the ACM/IEEE 14th International Conference on Cyber-Physical Systems (with CPS-IoT Week 2023)* (San Antonio, TX, USA) (ICCPs '23). Association for Computing Machinery, New York, NY, USA, 44–55. doi:10.1145/3576841.3585925
- [10] Qitong Gao et al. 2023. Offline Learning of Closed-Loop Deep Brain Stimulation Controllers for Parkinson Disease Treatment. In *Proceedings of the ACM/IEEE 14th International Conference on Cyber-Physical Systems (with CPS-IoT Week 2023)* (San Antonio, TX, USA) (ICCPs '23). Association for Computing Machinery, New York, NY, USA, 44–55. doi:10.1145/3576841.3585925
- [11] Aurélien Garivier and Eric Moulines. 2011. On Upper-Confidence Bound Policies for Switching Bandit Problems. In *Algorithmic Learning Theory*, Jyrki Kivinen, Csaba Szepesvári, Esko Ukkonen, and Thomas Zeugmann (Eds.). Springer Berlin Heidelberg, Berlin, Heidelberg, 174–188.
- [12] Hao-Lun Hsu, Qitong Gao, and Miroslav Pajic. 2024.  $\epsilon$ -Neural Thompson Sampling of Deep Brain Stimulation for Parkinson Disease Treatment. In *2024 ACM/IEEE 15th International Conference on Cyber-Physical Systems (ICCPs)*. 224–234. doi:10.1109/ICCPs61052.2024.00027
- [13] Ilija Jovanov et al. 2018. Platform for Model-Based Design and Testing for Deep Brain Stimulation. In *9th International Conference on Cyber-Physical Systems*. 263–274. doi:10.1109/ICCPs.2018.00033
- [14] Emilie Kaufmann, Olivier Cappe, and Aurelien Garivier. 2012. On Bayesian Upper Confidence Bounds for Bandit Problems. In *Proceedings of the Fifteenth International Conference on Artificial Intelligence and Statistics (Proceedings of Machine Learning Research, Vol. 22)*, Neil D. Lawrence and Mark Girolami (Eds.). PMLR, La Palma, Canary Islands, 592–600. <https://proceedings.mlr.press/v22/kaufmann12.html>
- [15] Abbas Kazerouni et al. 2017. Conservative contextual linear bandits. In *Proceedings of the 31st International Conference on Neural Information Processing Systems (Long Beach, California, USA) (NIPS'17)*. Curran Associates Inc., Red Hook, NY, USA, 3913–3922.
- [16] Tor Lattimore and Csaba Szepesvári. 2020. *Bandit Algorithms*. Cambridge University Press.
- [17] Scott F. Lempka et al. 2018. Characterization of the stimulus waveforms generated by implantable pulse generators for deep brain stimulation. *Clinical Neurophysiology* 129, 4 (2018), 731–742. doi:10.1016/j.clinph.2018.01.015
- [18] Xilin Liu et al. 2015. The PennBMBI: Design of a General Purpose Wireless Brain-Machine-Brain Interface System. *IEEE transactions on biomedical circuits and systems* 9 (03 2015). doi:10.1109/TBCAS.2015.2392555
- [19] Meili Lu et al. 2020. Application of Reinforcement Learning to Deep Brain Stimulation in a Computational Model of Parkinson's Disease. *IEEE Transactions on Neural Systems and Rehabilitation Engineering* 28, 1 (2020), 339–349. doi:10.1109/TNSRE.2019.2952637
- [20] C. Marras et al. 2018. Prevalence of Parkinson's disease across North America. *npj Parkinson's Disease* 4, 1 (10 Jul 2018), 21. doi:10.1038/s41531-018-0058-0
- [21] Brigitte Piallat et al. 2009. Monophasic but not biphasic pulses induce brain tissue damage during monopolar high-frequency deep brain stimulation. *Neurosurgery* 64 (2009), 156–162. doi:10.1227/01.NEU.0000336331.88559.CF
- [22] Marco Pirini et al. 2009. A computational modelling approach to investigate different targets in deep brain stimulation for Parkinson's disease. *Journal of Computational Neuroscience* 26, 1 (01 Feb 2009), 91–107. doi:10.1007/s10827-008-0100-z
- [23] Jonathan Rubin and David Terman. 2004. High Frequency Stimulation of the Subthalamic Nucleus Eliminates Pathological Thalamic Rhythmicity in a Computational Model. *J. Computational Neuroscience* 16 (2004), 211–35. doi:10.1023/B:JCNS.0000025686.47117.67
- [24] Muhammad Salam, Jose Perez-Velazquez, and Roman Genov. 2015. Seizure Suppression Efficacy of Closed-Loop Versus Open-Loop Deep Brain Stimulation in a Rodent Model of Epilepsy. *IEEE Transactions on Neural Systems and Rehabilitation Engineering* 24 (01 2015), 1–1. doi:10.1109/TNSRE.2015.2498973
- [25] Ruslana Shulyzki et al. 2015. 320-Channel Active Probe for High-Resolution Neuromonitoring and Responsive Neurostimulation. *IEEE Transactions on Biomedical Circuits and Systems* 9, 1 (2015), 34–49. doi:10.1109/TBCAS.2014.2312552
- [26] R.Q. So et al. 2012. Relative contributions of local cell and passing fiber activation and silencing to changes in thalamic fidelity during deep brain stimulation and lesioning: a computational modeling study. *J. Computational Neuroscience* 32, 3 (2012), 499–519. doi:10.1007/s10827-011-0366-4
- [27] S. Stanslaski et al. 2012. Design and Validation of a Fully Implantable, Chronic, Closed-Loop Neuromodulation Device With Concurrent Sensing and Stimulation. *IEEE transactions on neural systems and rehabilitation engineering : a publication of the IEEE Engineering in Medicine and Biology Society* 20 (01 2012), 410–21. doi:10.1109/TNSRE.2012.2183617
- [28] Scott Stanslaski et al. 2018. A Chronically Implantable Neural Coprocessor for Investigating the Treatment of Neurological Disorders. *IEEE Transactions on Biomedical Circuits and Systems* 12, 6 (2018), 1230–1245. doi:10.1109/TBCAS.2018.2880148
- [29] Fei Su et al. 2019. Model-Based Evaluation of Closed-Loop Deep Brain Stimulation Controller to Adapt to Dynamic Changes in Reference Signal. *Frontiers in Neuroscience* Volume 13 - 2019 (2019). doi:10.3389/fnins.2019.00956
- [30] George Thomas and Barbara Jobst. 2015. Critical review of the responsive neurostimulator system for epilepsy. *Medical Devices: Evidence and Research* 8 (10 2015), 405. doi:10.2147/MDER.S62853
- [31] Stavros Zanos et al. 2011. The Neurochip-2: An Autonomous Head-Fixed Computer for Recording and Stimulating in Freely Behaving Monkeys. *IEEE Transactions*

*on Neural Systems and Rehabilitation Engineering* 19 (2011), 427–435. <https://api.semanticscholar.org/CorpusID:20927653>

[32] Andy Zhou et al. 2017. WAND: A 128-channel, closed-loop, wireless artifact-free neuromodulation device. (08 2017). doi:10.48550/arXiv.1708.00556

[33] Dongruo Zhou, Lihong Li, and Quanquan Gu. 2020. Neural Contextual Bandits with UCB-based Exploration. In *Proceedings of the 37th International Conference on Machine Learning (Proceedings of Machine Learning Research, Vol. 119)*, Hal Daumé III and Aarti Singh (Eds.). PMLR, 11492–11502. <https://proceedings.mlr.press/v119/zhou20a.html>